J Sci Comput (2017) 71:1303–1318
DOI 10.1007/s10915-016-0340-4

A Second-Order Operator Splitting Fourier Spectral Method for Models of Epitaxial Thin Film Growth

Hyun Geun Lee[1] · **Jaemin Shin**[1] · **June-Yub Lee**[2]

Received: 15 July 2016 / Revised: 19 November 2016 / Accepted: 15 December 2016 /
Published online: 2 January 2017

Abstract In this paper, we develop an operator splitting Fourier spectral method for models of epitaxial thin film growth with and without slope selection. A main idea of the method is to split the original equation into linear and nonlinear parts, and then to evolve one step which consists of three substeps. The linear part is solved by the spectral method, which has a closed-form solution in the Fourier space. And the nonlinear part is also solved by the spectral method combined with the Crank–Nicolson type method. We numerically demonstrate that our method achieves spectral accuracy in space and second-order accuracy in time and alleviates restriction on the time step. We also perform long time simulations for the coarsening process to show the capability of the method.

Keywords Epitaxial thin film growth · Operator splitting method · Fourier spectral method · High-order accuracy

Mathematics Subject Classification 35Q99 · 65M12 · 65M70

1 Introduction

The epitaxial thin film growth model is the gradient flow of the following energy functional

$$\mathcal{E}(\phi) = \int_{\Omega} \left(F(\nabla\phi) + \frac{\delta}{2}|\Delta\phi|^2 \right) d\mathbf{x}, \tag{1}$$

This research was supported by the RP-Grant 2016 of Ewha Womans University and the Basic Science Research Program through the National Research Foundation of Korea (NRF) funded by the Korea government MOE (2009-0093827) and MSIP (2015-003037).

✉ June-Yub Lee
jyllee@ewha.ac.kr

[1] Institute of Mathematical Sciences, Ewha W. University, Seoul 120-750, Korea

[2] Department of Mathematics, Ewha W. University, Seoul 120-750, Korea

where Ω is a domain in $\mathbb{R}^d$ $(d = 1, 2, 3)$, $\phi : \Omega \to \mathbb{R}$ is a scaled height function of a thin film in a co-moving frame, $F(\nabla\phi)$ is a smooth function of its argument $\nabla\phi$, and δ is a constant. The first term, $\mathcal{E}_{\rm ES}(\phi) = \int_\Omega F(\nabla\phi)\, d\mathbf{x}$, models the Ehrlich–Schwoebel effect [1–3] where an adatom must overcome a higher energy barrier to stick to a step from an upper terrace. The second term, $\mathcal{E}_{\rm SD}(\phi) = \int_\Omega \frac{\delta}{2}|\Delta\phi|^2\, d\mathbf{x}$, models surface diffusion. There are two choices for $F(\nabla\phi)$ in $\mathcal{E}_{\rm ES}(\phi)$:

$$F_1(\nabla\phi) = \frac{1}{4}\left(|\nabla\phi|^2 - 1\right)^2 \quad \text{in [4]} \tag{2}$$

and

$$F_2(\nabla\phi) = -\frac{1}{2}\ln\left(1 + |\nabla\phi|^2\right) \quad \text{in [5].} \tag{3}$$

The L^2-gradient flows of (1) with $F_1(\nabla\phi)$ and $F_2(\nabla\phi)$ are

$$\frac{\partial\phi}{\partial t} = \nabla\cdot\left(|\nabla\phi|^2\,\nabla\phi\right) - \Delta\phi - \delta\Delta^2\phi \tag{4}$$

and

$$\frac{\partial\phi}{\partial t} = \nabla\cdot\left(\frac{|\nabla\phi|^2}{1+|\nabla\phi|^2}\,\nabla\phi\right) - \Delta\phi - \delta\Delta^2\phi, \tag{5}$$

respectively. $F_2(\nabla\phi)$ is bounded above and unbounded below. Furthermore, it has no relative minima, which implies that there are no energetically favored values for $|\nabla\phi|$. Physically this means that there is no slope selection mechanism. On the other hand, the model with $F_1(\nabla\phi)$ has a slope selection mechanism ($|\nabla\phi| = 1$ is preferred). For this reason, we call Eq. (4) the growth equation with slope selection and Eq. (5) the growth equation without slope selection. Equation (4) can be viewed as an approximation of Eq. (5) under the assumption that $|\nabla\phi|$ is small.

Recently, there have been many theoretical and numerical studies on the epitaxial thin film growth models (4) and (5). In [6], the well-posedness and solution regularity of the initial-boundary-value problem for Eq. (4) are proved. In [7], the well-posedness and solution regularity for Eqs. (4) and (5) are proved. The authors also prove bounds and error estimates for Galerkin spectral approximations. In [4,8,9], the difference between the interfacial dynamics governed by Eqs. (4) and (5) is investigated. Equation (4) predicts that pyramidal structures in the surface profile tend to have a uniform, constant mound slope [4,8]. On the other hand, Eq. (5) predicts an unbounded mound slope [9]. In [10], the authors apply Eyre's convex splitting idea [11] to Eqs. (4) and (5). A scheme proposed in [10] is first-order accurate in time and nonlinear due to the implicit treatment of the nonlinear term, and a second-order scheme based on the nonlinear convex splitting in [10] is proposed in [12]. In [10,12], the second-order central difference method is used for the space discretization. In [13], a linear iteration algorithm is presented to implement the second-order scheme in [12] for Eq. (5). In [14], the authors propose a first-order scheme for Eq. (5), which is based on a linear convex splitting. In [13,14], the spectral method is used for the space discretization.

The operator splitting method [15–20] can be applied to the epitaxial thin film growth models (4) and (5), which is to split the original equation into linear and nonlinear parts. It is theoretically proven [21–25] that one step evolution consisting of three substeps achieves second-order accuracy in time,

$$\phi(t+\Delta t) = \left(\mathcal{L}^{\Delta t/2}\circ\mathcal{N}^{\Delta t}\circ\mathcal{L}^{\Delta t/2}\right)\phi(t) + O(\Delta t^3), \tag{6}$$

when $\mathcal{L}$ and $\mathcal{N}$ are the exact solution operators for the linear and nonlinear parts of the original equation, respectively. In order to implement the operator splitting method, the exact solution operators $\mathcal{L}$ and $\mathcal{N}$ have to be replaced by their numerical approximations. The linear part can be easily solved by the spectral method which yields an exponentially accurate approximation to the solution operator $\mathcal{L}$. But there is a challenging problem how to numerically solve the nonlinear part with at least second-order accuracy in time in order to guarantee second-order accuracy of the operator splitting method (6). In [26], Cheng et al. solve the nonlinear part by the fourth-order central difference method combined with the third-order explicit Runge–Kutta method proposed in [27] and numerical experiments show that the proper constant time step should be of the order of $\delta/100$.

In this paper, we develop an operator splitting Fourier method for the epitaxial thin film growth models (4) and (5). The nonlinear part is also solved by the spectral method combined with the Crank–Nicolson type method which is known to be a stable second-order method in time. Thus our method alleviates restriction on the time step while maintaining spectral accuracy in space, which is a main contribution of our work. The convergence rate of our method is not proved theoretically but we numerically demonstrate that our method achieves spectral accuracy in space and second-order accuracy in time.

The aim of this paper is to provide a simple and efficient numerical method for the epitaxial thin film growth models (4) and (5). This paper is organized as follows. In Sect. 2, we propose a second-order operator splitting Fourier spectral method for the epitaxial thin film growth models (4) and (5). Numerical experiments are presented in Sect. 3. Finally, conclusions are drawn in Sect. 4.

2 Second-Order Operator Splitting Fourier Spectral Method

Equations (4) and (5) can be rewritten in the form

$$\frac{\partial \phi}{\partial t} = \nabla \cdot (G(|\nabla \phi|) \nabla \phi) - \Delta \phi - \delta \Delta^2 \phi, \tag{7}$$

where $G(s) = s^2$ for Eq. (4) and $G(s) = s^2/(1+s^2)$ for Eq. (5). We consider Eq. (7) in two-dimensional periodic space $\Omega = [0, L_1] \times [0, L_2]$ for simplicity of description. Let N_1 and N_2 be positive integers, $\Delta x = L_1/N_1$ and $\Delta y = L_2/N_2$ be the space step sizes, and Δt be the time step size. Let $\phi^n_{l_1 l_2}$ be an approximation of $\phi(x_{l_1}, y_{l_2}, t^n)$, where $x_{l_1} = l_1 \Delta x$ for $l_1 = 0, 1, \ldots, N_1 - 1$, $y_{l_2} = l_2 \Delta y$ for $l_2 = 0, 1, \ldots, N_2 - 1$, and $t^n = n \Delta t$.

For simplicity of notation, we define the "*linear operator*" $\mathcal{L}^{\Delta t}$ as follows:

$$\mathcal{L}^{\Delta t}(\phi(t^n)) := \phi(t^n + \Delta t),$$

where $\phi(t^n + \Delta t)$ is a solution of the linear equation

$$\frac{\partial \phi}{\partial t} = -\Delta \phi - \delta \Delta^2 \phi$$

with an initial condition $\phi(t^n)$. In order to solve Eq. (7) with the periodic boundary condition, we employ the discrete Fourier transform: for $k_1 = 0, 1, \ldots, N_1 - 1$, $k_2 = 0, 1, \ldots, N_2 - 1$, $\widehat{\phi}_{k_1 k_2} = \sum_{l_1=0}^{N_1-1} \sum_{l_2=0}^{N_2-1} \phi_{l_1 l_2} e^{-i(x_{l_1}\xi_{k_1} + y_{l_2}\xi_{k_2})}$, where $\xi_{k_1} = 2\pi k_1/L_1$ and $\xi_{k_2} = 2\pi k_2/L_2$. Then, we have an analytical formula for $\mathcal{L}^{\Delta t}$ in the discrete Fourier space

$$\mathcal{L}^{\Delta t}(\phi) = \mathcal{F}^{-1}\left[e^{A_{k_1 k_2} \Delta t} \mathcal{F}[\phi] \right],$$

where $A_{k_1k_2} = \left(\xi_{k_1}^2 + \xi_{k_2}^2\right) - \delta\left(\xi_{k_1}^2 + \xi_{k_2}^2\right)^2$ and $\mathcal{F}$ denotes the discrete Fourier transform and $\mathcal{F}^{-1}$ its inverse transform. We also define the "*nonlinear operator*" $\mathcal{N}^{\Delta t}$ as follows:

$$\mathcal{N}^{\Delta t}(\phi(t^n)) := \phi(t^n + \Delta t),$$

where $\phi(t^n + \Delta t)$ is a solution of the nonlinear equation

$$\frac{\partial \phi}{\partial t} = \nabla \cdot (G(|\nabla \phi|)\nabla \phi) \tag{8}$$

with an initial condition $\phi(t^n)$.

A second-order operator splitting method for Eq. (7) can be represented as

$$\phi^{n+1} = \left(\mathcal{L}^{\Delta t/2} \circ \mathcal{N}_2^{\Delta t} \circ \mathcal{L}^{\Delta t/2}\right)\phi^n, \tag{9}$$

where ϕ^n and ϕ^{n+1} are approximations of $\phi(t^n)$ and $\phi(t^n + \Delta t)$, respectively. In order to solve $\mathcal{N}_2^{\Delta t}$ with second-order accuracy, we apply the Crank–Nicolson type method to Eq. (8)

$$\frac{\phi^{n+1} - \phi^n}{\Delta t} = \nabla \cdot \left(G\left(\left|\nabla \phi^{n+\frac{1}{2}}\right|\right)\nabla \frac{\phi^{n+1} + \phi^n}{2}\right), \tag{10}$$

where $\phi^{n+\frac{1}{2}}$ is obtained by solving

$$\frac{\phi^{n+\frac{1}{2}} - \phi^n}{0.5\Delta t} = \nabla \cdot \left(G\left(|\nabla \phi^n|\right)\nabla \phi^{n+\frac{1}{2}}\right).$$

Equation (10) can be rewritten in the form

$$\mathbf{A}\phi^{n+1} = \phi^n + \frac{\Delta t}{2}\nabla \cdot \left(G\left(\left|\nabla \phi^{n+\frac{1}{2}}\right|\right)\nabla \phi^n\right), \tag{11}$$

where

$$\mathbf{A} = 1 + \frac{\Delta t}{2}\mathcal{F}^{-1}\left[\xi_{k_1}\mathcal{F}G\left(\left|\nabla \phi^{n+\frac{1}{2}}\right|\right)\mathcal{F}^{-1}\xi_{k_1} + \xi_{k_2}\mathcal{F}G\left(\left|\nabla \phi^{n+\frac{1}{2}}\right|\right)\mathcal{F}^{-1}\xi_{k_2}\right]\mathcal{F}.$$

The operator $\mathbf{A}$ is symmetric and positive definite, thus a fast solver such as the preconditioned conjugate gradient (PCG) method is used to solve the system (11).

The stopping criterion for the PCG iteration is that a relative residual is less than a tolerance (10^{-11} in this paper).

3 Numerical Experiments

In this section, we present examples (growth dynamics in 1D and 2D, and coarsening dynamics in 2D) for the epitaxial thin film growth models (4) and (5) to numerically demonstrate the accuracy and robustness of the proposed method. Here, we will see the evolution of the height function $\phi(\mathbf{x}, t)$, energy $\mathcal{E}(t)$, and roughness $w(t)$ which is defined by

$$w(t) = \sqrt{\frac{1}{|\Omega|}\int_\Omega \left(\phi(\mathbf{x}, t) - \bar{\phi}(t)\right)^2 d\mathbf{x}},$$

where $\bar{\phi}(t) = \frac{1}{|\Omega|}\int_\Omega \phi(\mathbf{x}, t)\, d\mathbf{x}$.

3.1 Growth Dynamics in 1D

We first demonstrate the convergence of the proposed method numerically. For the case with slope selection (4), we take an initial condition as

$$\phi(x,0) = 0.1\left(\sin\frac{\pi x}{2} + \sin\frac{2\pi x}{3} + \sin\pi x\right)$$

on a domain $\Omega = [0, 12]$. We set $\delta = 1$ and compute $\phi(x,t)$ for $0 < t \le T_f = 120$. This example was studied in [7] to observe the morphological instability due to the nonlinear interaction. In order to estimate the convergence rate with respect to Δt, simulations are performed by varying $\Delta t = 0.1 \cdot 2^{-10}, 0.1 \cdot 2^{-9}, \ldots, 0.1 \cdot 2$. We take the quadruply over-resolved numerical solution as the reference solution.

Figure 1 shows the evolution of the reference solution $\phi(x,t)$ with $\Delta x = 12/256$ for the case with slope selection (4). The initial oscillation is damped at $t = 1$. After a relatively long time, a new oscillation is generated, and then grows exponentially. The high-order perturbation analysis in [7] claims that high frequency modes with wavenumbers k_j larger than a critical wavenumber $k_c = \sqrt{1/\delta}$ in an initial condition decay exponentially fast and a new low frequency mode can be generated, whose wavenumber is a combination of k_j and is smaller than k_c. In this simulation, the critical wavenumber is $k_c = 1$ and the wavenumbers in the initial condition are 3, 4, and 6, thus the new oscillation in the steady state reached at $t = 60$ consists of only one sinusoidal profile.

The evolution of the energy $\mathcal{E}(t)$ and roughness $w(t)$ for the reference solution $\phi(x,t)$ is shown in Fig. 2. Initially both the energy and roughness decay rapidly. However, the roughness continues to grow for a relatively long time. Note that the flat end in Fig. 2 indicates that a steady state is reached. The results in Figs. 1 and 2 are in good agreement with those in [7].

For the case without slope selection (5), we take an initial condition as

$$\phi(x,0) = 0.1\left(\sin\frac{2\pi x}{3} + \sin\pi x + \sin\frac{4\pi x}{3}\right)$$

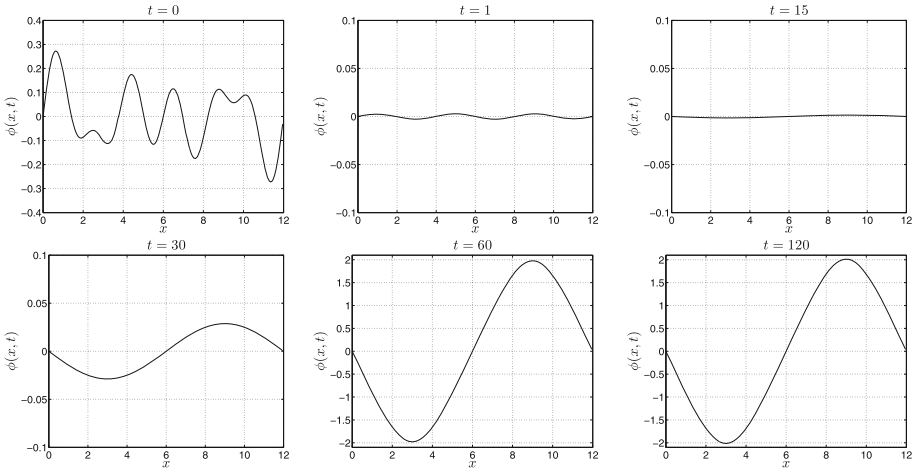

Fig. 1 Evolution of the reference solution $\phi(x,t)$ for the case with slope selection (4) for $\delta = 1$ with $\Delta x = 12/256$

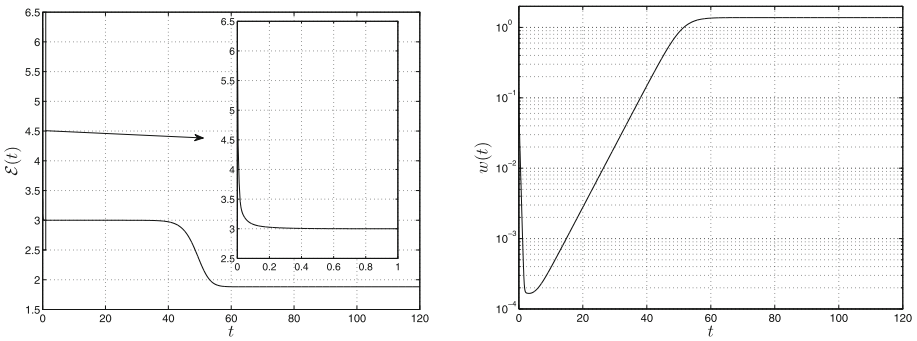

Fig. 2 Evolution of the energy (*left*) and roughness (*right*) for the reference solution $\phi(x, t)$ for the case with slope selection (4) for $\delta = 1$

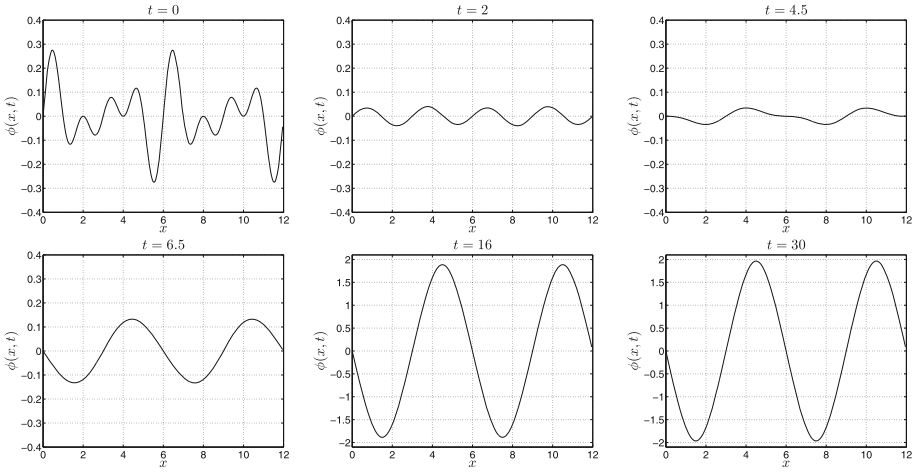

Fig. 3 Evolution of the reference solution $\phi(x, t)$ for the case without slope selection (5) for $\delta = 1/4$ with $\Delta x = 12/256$

on a domain $\Omega = [0, 12]$. We choose $\delta = 1/4$ to have slightly bigger k_c and compute $\phi(x, t)$ for $0 < t \leq T_f = 30$. Figures 3 and 4 show the evolution of the reference solution $\phi(x, t)$ with $\Delta x = 12/256$ and of $\mathcal{E}(t)$ and $w(t)$, respectively. Note that all the wavenumbers in the initial condition used in this simulation are 4, 6, and 8, and the critical wavenumber is 2. Thus the initial modes decay but a new mode with wavenumber 2 is generated.

For $\Delta x = 12/64,\ 12/256,\ 12/1024$, Fig. 5a, b show the relative l_2-errors of $\phi(x, t)$ for the cases with slope selection for $\delta = 1$ and without slope selection for $\delta = 1/4$ at different times for various time steps, respectively. For each grid size, the errors are computed by comparison with the reference solution. It is observed that the proposed method gives full spatial accuracy even with $\Delta x = 12/64$ and second-order time accuracy regardless of grid size.

3.2 Numerical Stability with Random Perturbation in 1D

In order to investigate the effect of δ on the growth dynamics, we consider the case with slope selection (4) with $\Delta t = 0.001$ and $\Delta x = 12/256$ on a domain $\Omega = [0, 12]$ and take an

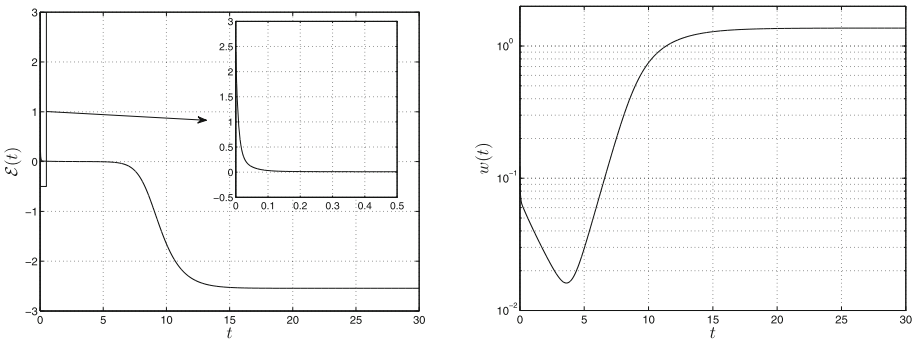

Fig. 4 Evolution of the energy (*left*) and roughness (*right*) for the reference solution $\phi(x,t)$ for the case without slope selection (5) for $\delta = 1/4$

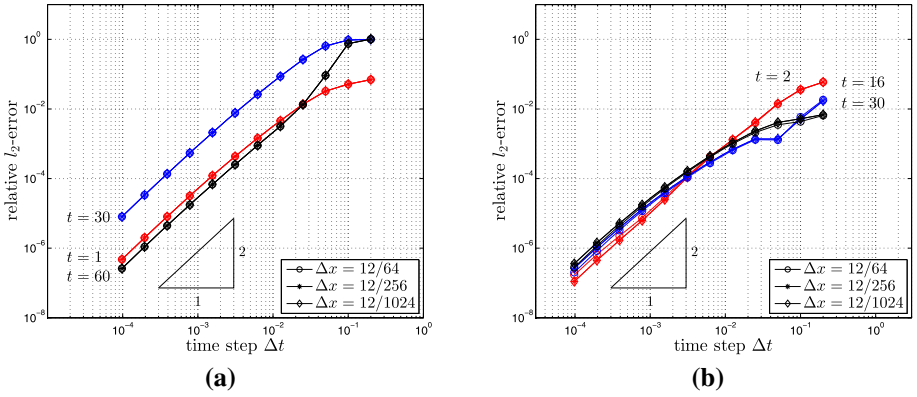

Fig. 5 Relative l_2-errors of $\phi(x,t)$ for the cases **a** with slope selection for $\delta = 1$ and **b** without slope selection for $\delta = 1/4$ at different times for various grid sizes and time steps

initial condition as $\phi(x,0) = \text{rand}(x)$, where rand$(x)$ is a random number between -0.2 and 0.2. Figure 6 shows the evolution of $\phi(x,t)$ and its energy $\mathcal{E}(t)$ for various δ. In each figure, the energy $\mathcal{E}(t)$ is omitted at $t = 0$ and plotted from $t = 0.001$. We observe that the high frequency modes in the initial condition decay exponentially fast and the remaining modes in the transient state evolve to relatively low frequency modes with wavenumber less than and equal to $\sqrt{1/\delta}$. This numerical test strongly suggests that spatial discretization size for a resolved computation must be chose depending on the smoothness of the initial data and $k_c = \sqrt{1/\delta}$.

Next, to demonstrate numerical stability of the proposed method, we consider the case with slope selection (4) with $\delta = 1$, $\Delta t = 0.001$, and $\Delta x = 12/256$ on a domain $\Omega = [0, 12]$. Two tests have been done: one with random perturbation of size η only at the initial step, and the other with random perturbation of size μ at every computational steps. First we add a random noise to a smooth test function $\phi_0(x,0) = 0.1\left(\sin\frac{\pi x}{2} + \sin\frac{2\pi x}{3} + \sin \pi x\right)$ for an initial condition,

$$\phi_\eta(x,0) = \phi_0(x,0) + \eta \cdot \text{rand}(x)\|\phi_0(x,0)\|_2, \tag{12}$$

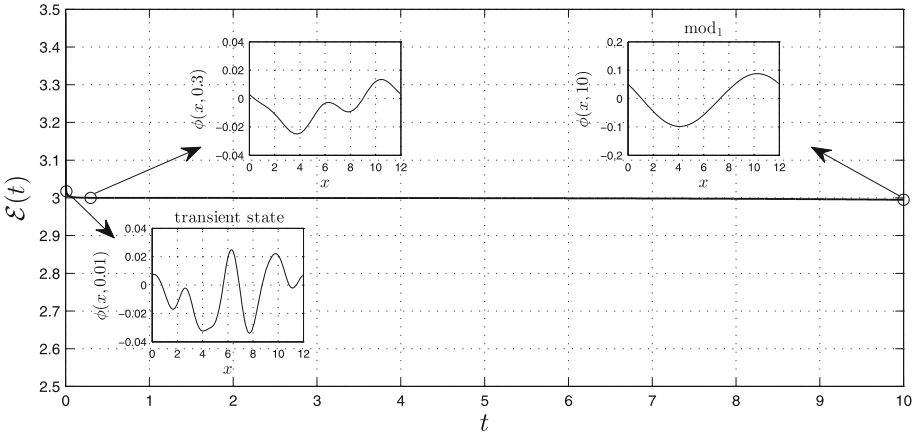

(a)

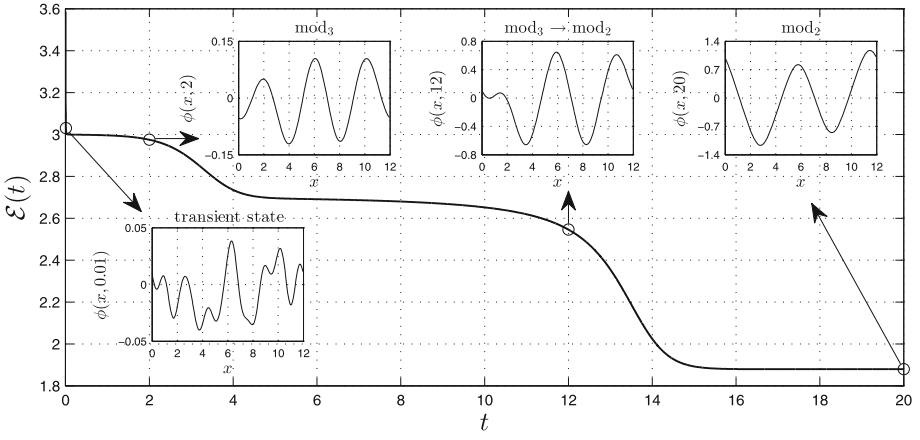

(b)

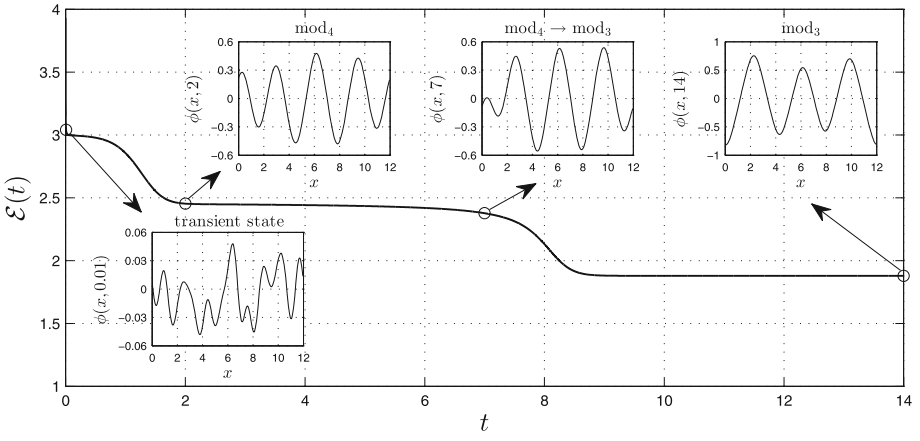

(c)

Fig. 6 Effect of δ on the growth dynamics $\phi(x,t)$ for the case with slope selection (4). In each figure, the energy $\mathcal{E}(t)$ is omitted at $t = 0$ and plotted from $t = 0.001$

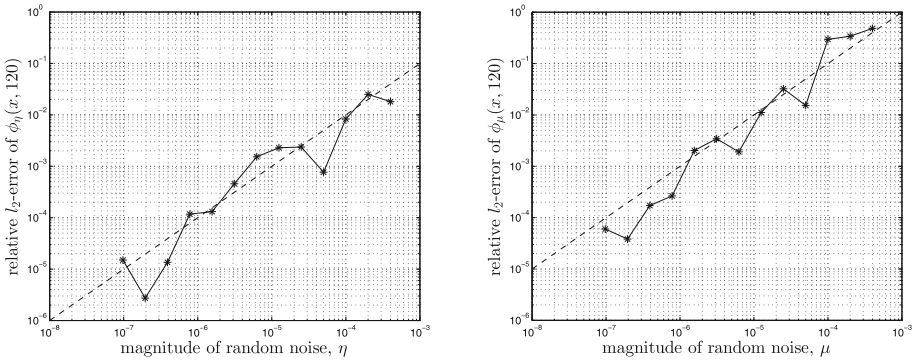

Fig. 7 Relative l_2-errors of **a** $\phi_\eta(x, 120)$ and **b** $\phi_\mu(x, 120)$ for the case with slope selection (4) for $\delta = 1$

where η is a magnitude of random noise and rand(x) is a random number with $\|\text{rand}(x)\|_2 = 1$. Figure 7a shows the relative l_2-errors of the computed solution, $\frac{\|\phi_\eta^n(x)-\phi_0^n(x)\|_2}{\|\phi_0^n(x)\|_2}$ for various η at $t^n = 120$.

And we also test a case with random perturbation at every computational steps using an initial condition $\phi_\mu(x, 0)$ chosen as in (12) and a random noise added to a computed solution at each time step,

$$\phi_\mu^{n+1}(x) = \left(\mathcal{L}^{\Delta t/2} \circ \mathcal{N}_2^{\Delta t} \circ \mathcal{L}^{\Delta t/2}\right)\left(\phi_\mu^n(x) + \mu \cdot \text{rand}(x)\|\phi_\mu^n(x)\|_2\right). \tag{13}$$

The relative l_2-errors of the computed solution, $\frac{\|\phi_\mu^n(x)-\phi_0^n(x)\|_2}{\|\phi_0^n(x)\|_2}$ for various μ at $t^n = 120$ are shown in Fig. 7b. The results in Fig. 7 indicate that the proposed method is linearly stable for a random noise.

We make a short remark on the numerical convergence of the proposed method before closing this subsection. In the previous subsection, we numerically show that the method is spectrally accurate in space and second-order consistent in time with smooth initial data. In this subsection, we also numerically demonstrate that the method is numerically stable for a random (high frequency) noise and the spatial discretization size for a resolved computation depends on $k_c = \sqrt{1/\delta}$. From the consistency and the stability, we believe that the method is convergent with spectral accuracy in space and second-order accuracy in time.

3.3 Growth Dynamics in 2D

Next, we consider the growth equations (4) and (5) in two-dimensional space. An initial condition is

$$\phi(x, y, 0) = 0.1\,(\sin 3x \sin 2y + \sin 5x \sin 5y)$$

on a domain $\Omega = [0, 2\pi] \times [0, 2\pi]$. We set $\delta = 0.1$ and compute $\phi(x, y, t)$ for $0 < t \le T_f = 30$. The grid size is fixed to $\Delta x = 2\pi/64$ which provides enough spatial accuracy. In order to estimate the convergence rate with respect to Δt, simulations are performed by varying $\Delta t = 0.01 \cdot 2^{-8}, 0.01 \cdot 2^{-7}, \ldots, 0.01$. We take the quadruply over-resolved numerical solution as the reference solution.

Figures 8 and 9 show the evolution of the reference solution $\phi(x, y, t)$ and of $\mathcal{E}(t)$ and $w(t)$ for the case with slope selection (4), respectively. The initial condition consists of two

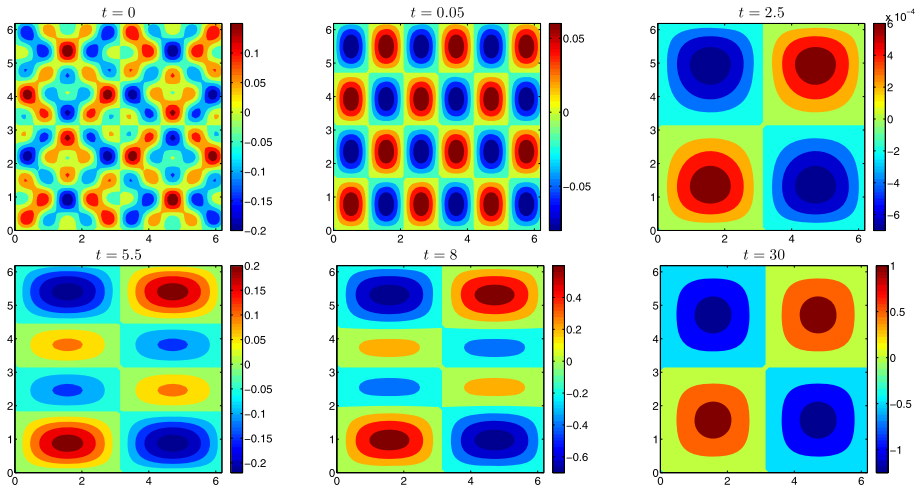

Fig. 8 Evolution of the reference solution $\phi(x, y, t)$ for the case with slope selection (4) for $\delta = 0.1$

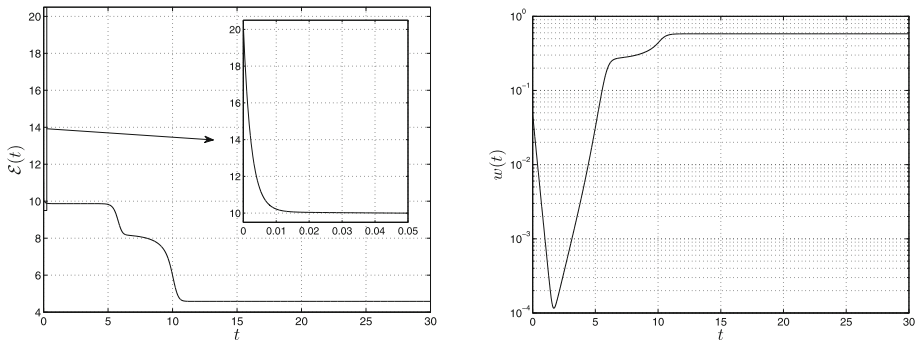

Fig. 9 Evolution of the energy (*left*) and roughness (*right*) for the reference solution $\phi(x, y, t)$ for the case with slope selection (4) for $\delta = 0.1$

modes $\text{mod}_{3,2}$ and $\text{mod}_{5,5}$. One of these modes, $\text{mod}_{5,5}$, disappears at $t = 0.05$. At $t = 2.5$, both of these modes disappear but a new mode is generated. Another new mode appears at $t = 5.5$ but this mode almost disappears at $t = 8$. At $t = 30$, we can see a steady state which consists of only one mode $\text{mod}_{1,1}$.

Similar growth dynamics is observed in the case without slope selection (5) (see Figs. 10 and 11). In particular, the initial rough-smooth-rough pattern is the same. However, the height ϕ for the case without slop selection is larger in magnitude than that for the case with slope selection, and the energy becomes negative. The results in Figs. 8, 9, 10 and 11 are in good agreement with those in [7].

Figure 12a, b show the relative l_2-errors of $\phi(x, y, t)$ for the cases with and without slope selection at $t = 0.05,\ 8,\ 30$ for various time steps, respectively. Here, the errors are computed by comparison with the reference solution. It is observed that the proposed method gives second-order accuracy in time.

The number of the PCG iterations with $\Delta t = 0.005$ and 0.01 for the case with slope selection (4) is shown in Fig. 13. For large time step, the number of the PCG iterations is within 10, and thus the CPU times consumed in our algorithm are cheap (68.5 and 47.2 (Sec)

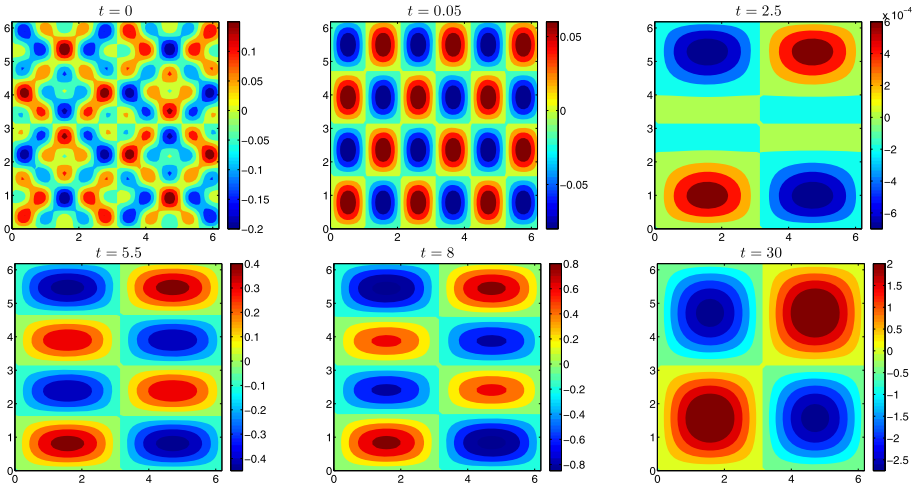

Fig. 10 Evolution of the reference solution $\phi(x, y, t)$ for the case without slope selection (5) for $\delta = 0.1$

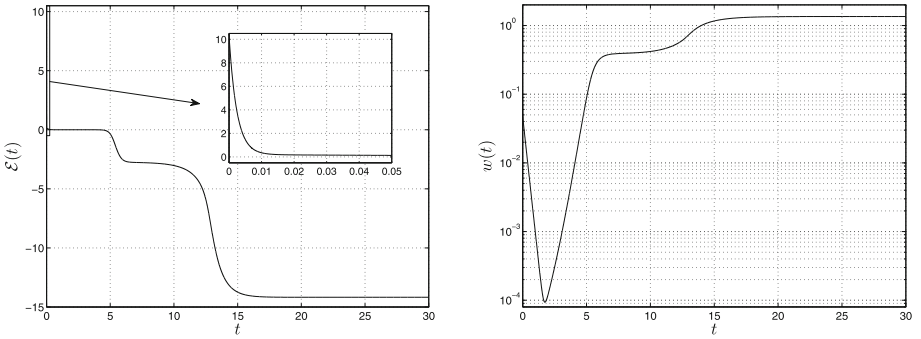

Fig. 11 Evolution of the energy (*left*) and roughness (*right*) for the reference solution $\phi(x, y, t)$ for the case without slope selection (5) for $\delta = 0.1$

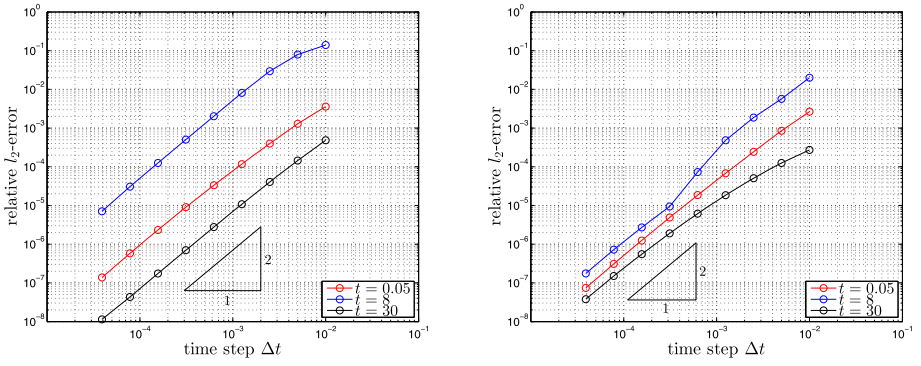

Fig. 12 Relative l_2-errors of $\phi(x, y, t)$ for the cases **a** with and **b** without slope selection for $\delta = 0.1$ at $t = 0.05,\ 8,\ 30$ for various time steps

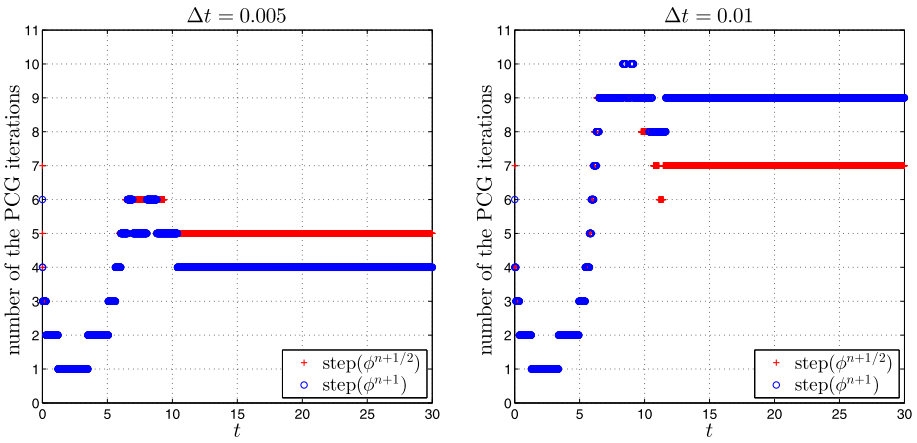

Fig. 13 Number of the PCG iterations for the case with slope selection (4) for $\delta = 0.1$

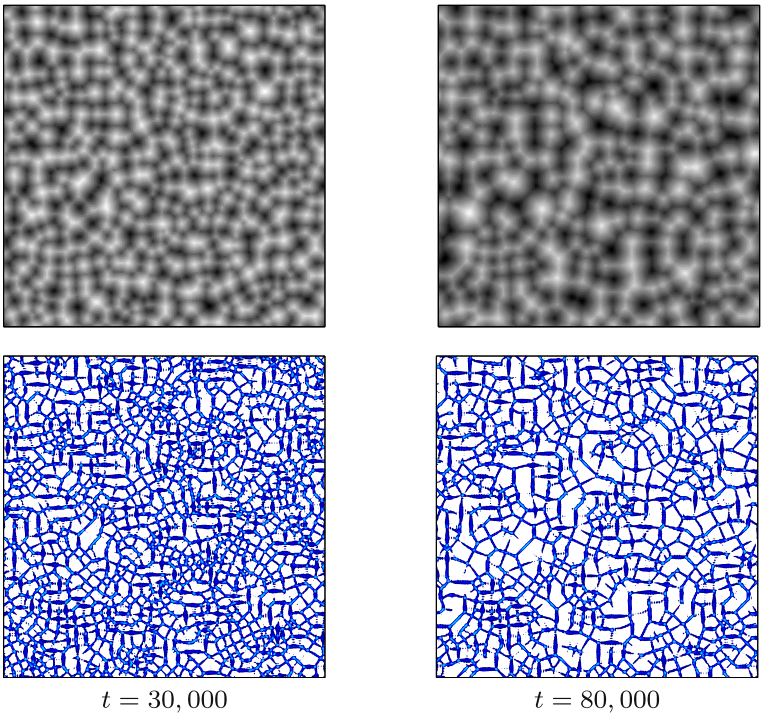

Fig. 14 The solution ϕ ranging $[-45, 45]$ (*top*) and contour plots of the free energy F_{free} (*bottom*) for the case with slope selection (4) for $\delta = 1$

for $\Delta t = 0.005$ and 0.01, respectively, using MATLAB 7.14 on a machine with 3.2 GHz Intel i5 CPU and 4 GB memory).

3.4 Coarsening Dynamics in 2D

With slope selection, the growth equation (4) predicts $\mathcal{E}(t) \sim O(t^{-1/3})$ and $w(t) \sim O(t^{1/3})$ as $t \to \infty$. Likewise, without slope selection, the growth equation (5) predicts $\mathcal{E}(t) \sim$

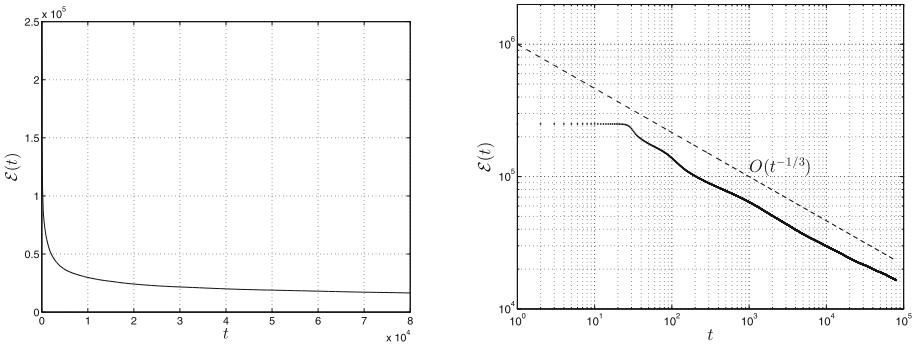

Fig. 15 $t^{-1/3}$ energy decay rate for the case with slope selection (4) for $\delta = 1$. The *dots* represent the plots obtained by the numerical simulation

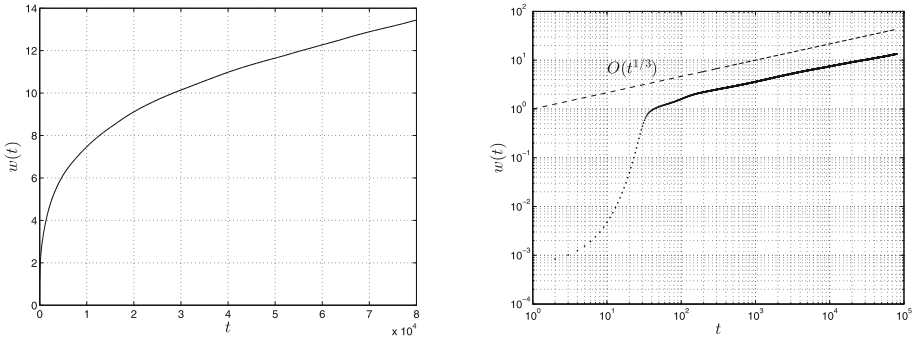

Fig. 16 $t^{1/3}$ roughness growth rate for the case with slope selection (4) for $\delta = 1$. The *dots* represent the plots obtained by the numerical simulation

$O(-\ln(t))$ and $w(t) \sim O(t^{1/2})$ as $t \to \infty$. (See [7,8,28] and reference therein). In order to compare our numerical solutions with the predicted energy decay and roughness growth rates, we take an initial condition as $\phi(x, y, 0) = \text{rand}(x, y)$ on a domain $\Omega = [0, 1000] \times [0, 1000]$. Here, $\text{rand}(x, y)$ is a random number between -0.001 and 0.001, and we use $\delta = 1$, $\Delta x = 1000/256$, and $\Delta t = 1$.

For the case with slope selection (4), Fig. 14 shows the solution ϕ and the contour lines of the free energy $F_{\text{free}}(\mathbf{x}, t)$ at $t = 30,000$ and $80,000$, where F_{free} is defined by

$$F_{\text{free}} = \frac{1}{4}\left(|\nabla\phi|^2 - 1\right)^2 + \frac{\delta}{2}|\Delta\phi|^2.$$

The free energy is concentrated on the edges of the pyramidal structures and the pyramids grow in time via a coarsening process. These results are in good agreement with those in [8,26,29]. Figures 15 and 16 show the evolution of the energy $\mathcal{E}(t)$ and roughness $w(t)$, respectively. The energy decays like $t^{-1/3}$ and the roughness grows like $t^{1/3}$, which match the results in [7,8,28].

For the case without slope selection (5), Figs. 17, 18 and 19 show the solution ϕ and the contour lines of $F_{\text{free}}(\mathbf{x}, t)$, the decay of $\mathcal{E}(t)$, and the growth of $w(t)$, respectively, where F_{free} is defined by

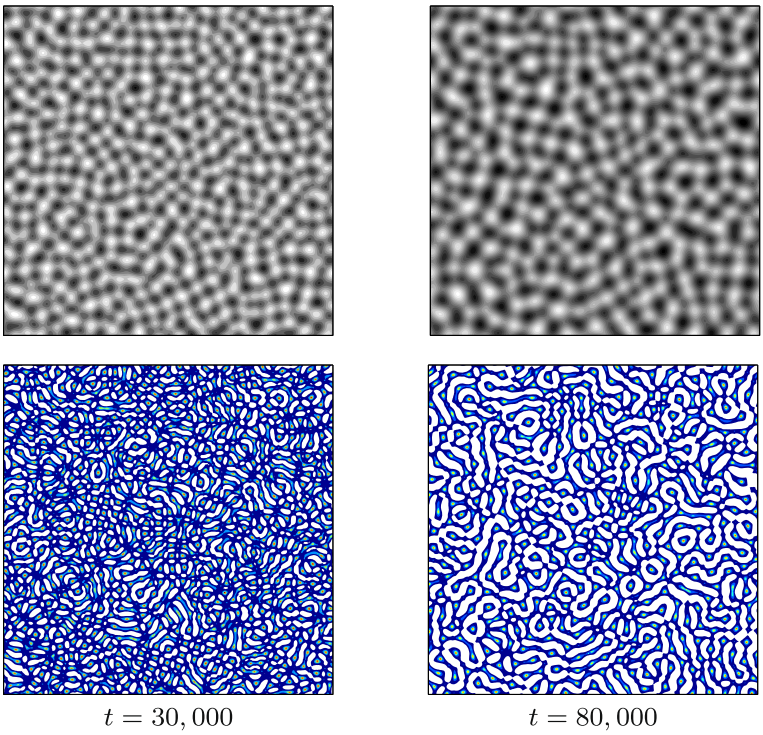

Fig. 17 The solution ϕ ranging $[-350, 350]$ (*top*) and contour plots of F_{free} (*bottom*) for the case without slope selection (5) for $\delta = 1$

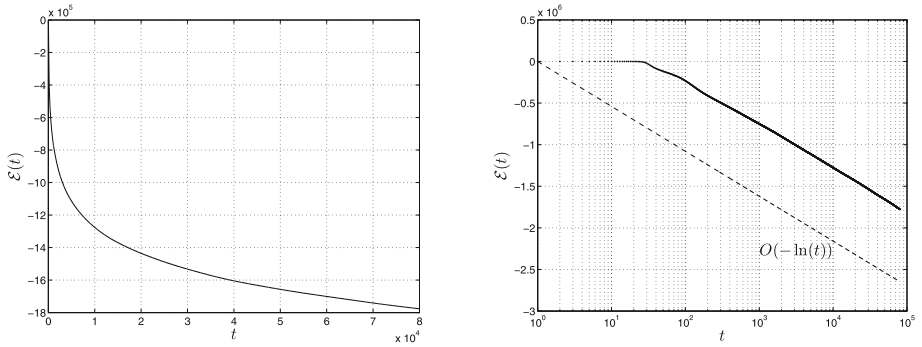

Fig. 18 $-\ln(t)$ energy decay rate for the case without slope selection (5) for $\delta = 1$. The *dots* represent the plots obtained by the numerical simulation

$$F_{\text{free}} = -\frac{1}{2}\ln\left(1 + |\nabla\phi|^2\right) + \frac{\delta}{2}|\Delta\phi|^2.$$

The energy decays like $-\ln(t)$ and the roughness grows like $t^{1/2}$, which match the results in [7,8,28].

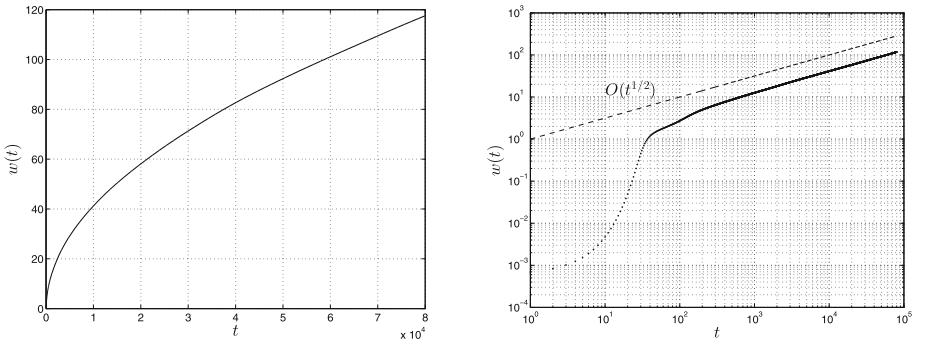

Fig. 19 $t^{1/2}$ roughness growth rate for the case without slope selection (5) for $\delta = 1$. The *dots* represent the plots obtained by the numerical simulation

4 Conclusions

We developed the operator splitting Fourier spectral method for models of epitaxial thin film growth with and without slope selection. The main idea of the method was to split the original equation into linear and nonlinear parts, and then to evolve one step which consists of three substeps: $\phi^{n+1} = \left(\mathcal{L}^{\Delta t/2} \circ \mathcal{N}_2^{\Delta t} \circ \mathcal{L}^{\Delta t/2}\right) \phi^n$. Both linear and nonlinear parts were solved by the spectral method. We numerically demonstrated that the method gives full spatial accuracy and second-order time accuracy. We also performed long time simulations for the coarsening process, where the energy decay and roughness growth rates ($t^{-1/3}$ and $t^{1/3}$ for the case with slope selection, and $-\ln(t)$ and $t^{1/2}$ for the case without slope selection) can be observed clearly.

In the present work, the convergence rate of the method was only shown numerically. Thus, in future work, we plan to analyze the convergence rate of the method theoretically.

References

1. Ehrlich, G., Hudda, F.G.: Atomic view of surface self-diffusion: Tungsten on tungsten. J. Chem. Phys. **44**, 1039–1049 (1966)
2. Schwoebel, R.L., Shipsey, E.J.: Step motion on crystal surfaces. J. Appl. Phys. **37**, 3682–3686 (1966)
3. Schwoebel, R.L.: Step motion on crystal surfaces. II. J. Appl. Phys. **40**, 614–618 (1969)
4. Ortiz, M., Repetto, E.A., Si, H.: A continuum model of kinetic roughening and coarsening in thin films. J. Mech. Phys. Solids **47**, 697–730 (1999)
5. Johnson, M.D., Orme, C., Hunt, A.W., Graff, D., Sudijono, J., Sander, L.M., Orr, B.G.: Stable and unstable growth in molecular beam epitaxy. Phys. Rev. Lett. **72**, 116–119 (1994)
6. King, B.B., Stein, O., Winkler, M.: A fourth-order parabolic equation modeling epitaxial thin film growth. J. Math. Anal. Appl. **286**, 459–490 (2003)
7. Li, B., Liu, J.-G.: Thin film epitaxy with or without slope selection. Eur. J. Appl. Math. **14**, 713–743 (2003)
8. Moldovan, D., Golubović, L.: Interfacial coarsening dynamics in epitaxial growth with slope selection. Phys. Rev. E **61**, 6190–6214 (2000)
9. Golubović, L.: Interfacial coarsening in epitaxial growth models without slope selection. Phys. Rev. Lett. **78**, 90–93 (1997)
10. Wang, C., Wang, X., Wise, S.M.: Unconditionally stable schemes for equations of thin film epitaxy. DCDS-A **28**, 405–423 (2010)
11. Eyre, D.: Unconditionally gradient stable time marching the Cahn–Hilliard equation. MRS Proc. **529**, 39–46 (1998)

12. Shen, J., Wang, C., Wang, X., Wise, S.M.: Second-order convex splitting schemes for gradient flows with Ehrlich–Schwoebel type energy: application to thin film epitaxy. SIAM J. Numer. Anal. **50**, 105–125 (2012)
13. Chen, W., Wang, C., Wang, X., Wise, S.M.: A linear iteration algorithm for a second-order energy stable scheme for a thin film model without slope selection. J. Sci. Comput. **59**, 574–601 (2014)
14. Chen, W., Conde, S., Wang, C., Wang, X., Wise, S.M.: A linear energy stable scheme for a thin film model without slope selection. J. Sci. Comput. **52**, 546–562 (2012)
15. Strang, G.: On the construction and comparison of difference schemes. SIAM J. Numer. Anal. **5**, 506–517 (1968)
16. Chertock, A., Doering, C.R., Kashdan, E., Kurganov, A.: A fast explicit operator splitting method for passive scalar advection. J. Sci. Comput. **45**, 200–214 (2010)
17. Lee, H.G., Lee, J.-Y.: A semi-analytical Fourier spectral method for the Allen–Cahn equation. Comput. Math. Appl. **68**, 174–184 (2014)
18. Lee, H.G., Lee, J.-Y.: A second order operator splitting method for Allen–Cahn type equations with nonlinear source terms. Phys. A **432**, 24–34 (2015)
19. Lee, H.G., Shin, J., Lee, J.-Y.: First and second order operator splitting methods for the phase field crystal equation. J. Comput. Phys. **299**, 82–91 (2015)
20. Kao, C.-Y., Kurganov, A., Qu, Z., Wang, Y.: A fast explicit operator splitting method for modified Buckley–Leverett equations. J. Sci. Comput. **64**, 837–857 (2015)
21. Jahnke, T., Lubich, C.: Error bounds for exponential operator splittings. BIT Numer. Math. **40**, 735–744 (2000)
22. Lubich, C.: On splitting methods for Schrödinger–Poisson and cubic nonlinear Schrödinger equations. Math. Comput. **77**, 2141–2153 (2008)
23. Chertock, A., Kurganov, A., Petrova, G.: Fast explicit operator splitting method for convection-diffusion equations. Int. J. Numer. Methods Fluids **59**, 309–332 (2009)
24. Holden, H., Karlsen, K.H., Risebro, N.H., Tao, T.: Operator splitting for the KdV equation. Math. Comput. **80**, 821–846 (2011)
25. Holden, H., Lubich, C., Risebro, N.H.: Operator splitting for partial differential equations with Burgers nonlinearity. Math. Comput. **82**, 173–185 (2013)
26. Cheng, Y., Kurganova, A., Qu, Z., Tang, T.: Fast and stable explicit operator splitting methods for phase-field models. J. Comput. Phys. **303**, 45–65 (2015)
27. Medovikov, A.A.: High order explicit methods for parabolic equations. BIT Numer. Math. **38**, 372–390 (1998)
28. Li, B., Liu, J.-G.: Epitaxial growth without slope selection: energetics, coarsening, and dynamic scaling. J. Nonlinear Sci. **14**, 429–451 (2004)
29. Xu, C., Tang, T.: Stability analysis of large time-stepping methods for epitaxial growth models. SIAM J. Numer. Anal. **44**, 1759–1779 (2006)